https://dx.doi.org/10.21577/0103-5053.20220086

J. Braz. Chem. Soc., Vol. 34, No. 1, 36-53, 2023

Article

Evaluation of the Properties of $LaNiO_3$ Material Prepared by the Modified Proteic Method for Adsorption of Environmental Contaminants

Jéssica A. S. Lemos,[a] Iasmin A. Ribeiro,[a] Marcelo J. B. Souza[b] and Anne M. Garrido Pedrosa *,[a]*

[a]*Programa de Pós-Graduação em Química, Universidade Federal de Sergipe, Av. Marechal Rondon, Rosa Elze, 49100-000 São Cristóvão-SE, Brazil*

[b]*Programa de Pós-Graduação em Engenharia Química, Universidade Federal de Sergipe, Av. Marechal Rondon, Rosa Elze, 49100-000 São Cristóvão-SE, Brazil*

$LaNiO_3$ material was synthesized by modified proteic method, calcined at 900 °C/2 h in air atmosphere and was applied to remove environmental contaminants. $LaNiO_3$ phase with a perovskite structure was formed in the calcined material, which has a surface area of 22 m^2 g^{-1} and is formed by fine particles agglomerated, with pH of the zero charge point of 7.44. The removal of a model pollutant (Turquoise Blue dye) indicated that the better removal occurs in acidic pH and with adsorbent's mass of 50 mg, showing average value around 90% of removal efficiency and 131 mg g^{-1} for adsorption capacity (q) value. The variable constants model was the one that best fit the kinetic. $LaNiO_3$ material resisted the test conditions and the recovery process, and maintained its high adsorption capacity throughout the six regeneration cycles studied, which indicates that it is a promising material as an adsorbent of pollutants and does not generate waste during the process.

Keywords: perovskite structure, lanthanum nickelate, synthesis with collagen, removal of environmental contaminants

Introduction

The increasing population has exposed the environment to various forms of contamination. Among the most worrying are water bodies, where the indiscriminate use of water by the population, and significant amounts of untreated chemical residues present in it have made it increasingly scarce and unsuitable for human consumption.[1]

Currently, textile effluents are classified among substances considered harmful to the environment.[2] Characterized by being highly colored due to the presence of dyes, the effluent upon reaching the rivers causes a reduction in the penetration of sunlight, which ends up decreasing the photosynthetic activity, the concentration of dissolved oxygen and the quality of the water.[3] In addition, textile effluents have a high chemical and biological oxygen demand (COD and BOD), high alkalinity and intense coloring due to the presence of dyes, which are thermally and chemically stable, and may exhibit acute toxicity and be carcinogenic and/or mutagens.[4]

Textile dyes are organic compounds that have complex aromatic structures, usually consisting of a chromophore group, responsible for color, and auxiliary groups, responsible for fixation. Among these, we highlight the class of reactive dyes, such as the Turquoise Blue dye, which has as characteristic one or more groups –N=C– linked to aromatic systems and which act in the fixation of fibers.[5,6] Dyes are compounds that are of great importance for the industrial sector, which are capable of causing great fascination in humanity for the beauty and perfection of colors. They are used in several industrial segments such as in the food, cosmetic and textile sectors.[7,8]

The removal of dyes through conventional physical, chemical and biological treatments has been increasingly hampered by the thermal and chemical stability of dyes. Therefore, the application of the adsorption technique and the use of new materials have been studied in order to minimize or eliminate these contaminants from water bodies. Removal from solid/solution interfaces is an important way of controlling the increase in pollution of natural waters with dyes.[9]

In order to obtain good performance in any adsorption process, it is essential to choose an adsorbent material that has characteristics such as high adsorption capacity, easy

*e-mail: annemgp@gmail.com
Editor handled this article: Fernando C. Giacomelli (Associate)

availability, high selectivity, low cost, long useful life and regeneration capacity so its use can be considered viable.[10]

Currently, there is a range of natural or synthetic materials being used as adsorbents, such as zeolites, activated carbon, oxides, silica, among others. Table 1 shows some results found in the literature on the removal of the Turquoise Blue dye using different materials. It is worth mentioning that these studies showed satisfactory removal efficiency, and for the vast majority, the balance time was short.

In view of the data in Table 1, it is noted that oxides have gained a strong presence in the removal of the Turquoise Blue dye, presenting satisfactory results in removal efficiency, as well as a short equilibrium time when compared to other materials. In addition, the high regeneration capacity of this class has made it an advantage over other materials. Thus, the class of mixed oxides with perovskite structure can present interesting results when the subject is the adsorption of dyes.

The perovskite structure is a common structure of several mixed oxide that present the general formula ABX_3, where position A is occupied by metal ions that have large ionic rays such as alkali metals, alkaline earth and rare earths, position B is occupied by smaller ions like those of the transition metals of d block and X is mostly O^{2-}, although perovskites containing nitride, hydride and halogenated metal can also be synthesized.[20,21] Generally, metal that occupies position A provides mechanical resistance to perovskites, while the metal that occupies position B improves reactivity in redox processes.[22,23]

Research involving materials with perovskite structure have been considered as multifunctional materials exhibiting magnetic, electrical, catalytic, optical and adsorptive properties, among others, and are also easily synthesized.[24-27] The efficiency of these materials in specific applications can be related to several factors, including the partial doping of the metal that occupies site A and the synthesis method employed.[28] For this reason, the development of new materials is essential to associate the effect of experimental measures with their properties and applications. Among the main synthetic methods are the Pechini method, combustion, mechanosynthesis, co-precipitation, solgel and the chelating precursor method.[25,26] In addition, heat treatments at high temperatures after the initial stages of synthesis are generally necessary for the formation of the desired perovskite phase.[23]

Different synthesis routes have been developed in recent years in order to produce materials with better characteristics such as: larger surface areas, greater crystallinity, smaller crystallites, etc. All of these proposed routes are aimed at producing structures that contribute to the development of materials with perovskite structure with the best characteristics in order to be used in specific reactions/process.[29]

The $LaNiO_3$ material with perovskite structure, according to literature data, presents a wide range of applications, varying its method of synthesis and experimental conditions, for example, temperature and calcination time. Table 2 lists scientific works with different synthesis routes, characteristics and applications of the $LaNiO_3$ material. According to Table 2, it is noted that most of the synthesized materials have a rhombohedral crystalline structure, which is one of the most common

Table 1. Materials applied to remove the Turquoise Blue dye and experimental conditions

Material	M_a / mg	V_s / mL	pH	C / (mg L^{-1})	E_R / %	q / (mg g^{-1})	Equilibrium time / h	Reference
MTW zeolite	50	50	1.0	50	83	–	0.8	11
Commercial activated carbon	6000	1000	2.0	500	–	120	30.0	12
Activated carbon (pods) with zinc chloride	50	50	2.0	20	78	–	1.7	13
Diatomite	–	–	2.0	500	63	–	1.0	14
Reticulated laccase with chitosan	10	100	4.5	–	74	–	72.0	15
TiO_2	800	500	7.0	50	80	–	3.5	16
Cashew bagasse	5000	1000	2.0	200	57	–	2.5	17
SiO_2	50	50	6.0	200	–	44	1.3	18
Si-Fe_2O_3	50	50	8.0	200	–	46	1.3	18
Free bacteria	–	–	7.0	50	96	120	24	19
Bacteria immobilized by polylactic acid electrospinning	–	–	7.0	50	90	112	24	19
Bacteria immobilized by polycaprolactone electrospinning	–	–	7.0	5	88	110	24	19

M_a: adsorbent mass; V_s: solution volume; C: solution concentration; E_R: efficiency removal; q: amount of dye adsorbed; MTW: Mobil twelve.

in relation to the distortion of the perfect cubic structures of the perovskites. In addition, it is possible to perceive the variety of applications of this type of material that encompass different properties, including catalysis, adsorption, biomedical tests, among others. The $LaNiO_3$ show antimicrobial activity without causing toxic effect on mammalian cell.[30]

The modified protein method is derived from the proteic sol-gel method. This method has characteristics such as: the low cost, the efficiency in obtaining crystalline materials of high purity, the use of low processing temperatures, as well as the formation of monophasic nanostructured oxides, which present an adequate surface area and smaller grains. All these characteristics make this method relevant in the production of materials with a perovskite type structure.[40,41] Many organic agents have been useful in the precipitation of metals due to their sensitivity and their potential for selectivity when reacting with metal ions. The most useful organic reagents form chelate-type complexes with metal ions.[8] Literature studies[36,41] report that the synthesis of $LaNiO_3$-type perovskites using collagen and soy protein as a chelating agent obtained good results when compared to conventional methods.

The treatment of water to remove dyes can be carried out by some physical, chemical and/or biological processes. Studies focusing on the use of mixed oxides with adsorptive properties for dye removal are still scarce in the literature, however there are good results in the use of $Ni_{0.5}Zn_{0.5}Fe_2O_4$ ferrite, $LaNiO_3$ and $LaMnO_3$ as adsorbents in the removal of Congo Red dye.[25,36,37] Recently, the degradation of Reactive Black 5 dye has been reported through the catalytic oxidation process using the $LaNiO_3$ material as a catalyst. In such work, a degradation of 65% was obtained in a time of 120 min.[42] The degradation of the Methylene Blue dye was also verified through the photocatalysis process. In this work, a material with a $CaTiO_3$ perovskite structure was used, showing excellent results for the concentration of 10 mg L^{-1}, reaching 89.4% of decomposition efficiency.[43] Table 3 shows works reported in the literature in which materials synthesized with perovskite structure are applied in the removal of dyes. It is observed that there are a variety of dyes, which are removed by different processes.

From the data in Table 3, it can be seen that the removal of dyes by the adsorption process presents satisfactory results when compared to other processes. In addition, adsorption is a low-energy, easy-to-operate, high-color removal process that provides the possibility of regenerating the adsorbent material. Among the studies shown in Table 3, only a few of those that use adsorption present studies on the reuse or regeneration of the adsorbent material.

Table 2. Different synthesis routes, characteristics and applications of $LaNiO_3$ material

Synthesis conditions			Main features			Application	Reference
SM	Temperature / °C	time / h	CS	SSA / (m^2 g^{-1})	CR / nm		
Sol-gel combustion	175	5 min	rhombohedral perovskite	9.2	46	antibacterial activity	30
Self-combustion	700	4	rhombohedral perovskite	9.0	–	dry methane reform catalyst in synthesis gas	31
Sol-gel	700	5	rhombohedral perovskite	7.9	–	high performance supercapacitor electrodes and anodes and lithium ion battery	32
Hydrothermal	650	2	–	–	–	biomedical trials	33
Electrospinning	700	2	rhombohedral perovskite	12.0	–	catalysts for zinc-air rechargeable batteries	34
Self-combustion	800	3	rhombohedral perovskite	–	–	dye adsorption	35
Modified protein	700 900	2	rhombohedral perovskite	82.0 90.0	–	dye adsorption	36
Mechano-synthesis	700 900	2	rhombohedral perovskite	44.0 32.0	6 6	dye adsorption	37
Microwave-assisted citrate	900	10	rhombohedral perovskite	–	–	electrocatalyst for glycerol oxidation	38
Hydrothermal	600 700 800	2	rhombohedral perovskite	–	14.2 17.9 20.9	microwave absorber	39

SM: synthesis method; CS: crystalline structure; SSA: specific surface area; CR: crystallite size.

It should be noted that in addition to the development of suitable materials for removing dyes from the aquatic environment, it is also essential to give a correct destination to the material generated after the adsorption process. An appropriate strategy in this scenario would involve both the disposal of the residue and the possible recovery of the adsorbents for reuse.

Some works in the literature have studied the destination of the material generated after the removal process. In one of them,[48] the perovskite $LaFeO_3$ regeneration experiment after the adsorption of Rhodamine B dye was carried out by pyrolysis at 580 °C for 20 min. This adsorption-desorption progress was made and it was found that the removal efficiency value decreased from 99% to approximately 96%, suggesting that pyrolysis was an efficient approach for the regeneration of the material under study and this type of adsorbent can be reused repeatedly to remove the dye.[48]

Another study[37] using the perovskite structures $LaMnO_3$ and $LaNiO_3$ also showed a possibility of regeneration of the adsorbent after the adsorption of the Congo Red dye. In this work, the material resulting from the adsorption is calcined at 900 °C for 2 h and is characterized by the techniques of X-ray diffractometry (XRD), Fourier transform infrared spectroscopy (FTIR) and thermogravimetry analysis (TGA) indicating the possible adsorption of the dye and the recovery of the synthesized perovskites when this temperature is used to degrade the impregnated dye. It is worth mentioning that in this work, a new test is not carried out after the adsorbent recovery procedure.[37]

This article describes the study of the $LaNiO_3$ material with perovskite structure synthesized by the modified proteic method with collagen as the chelating agent. In addition, it also assesses the viability of the obtained material as an adsorbent to remove environmental contaminants, such as dyes, in aqueous media with promising results, which is a recent application for this class of materials. The study is also focused on the recovery and reuse of $LaNiO_3$ material.

Experimental

Synthesis of $LaNiO_3$ material

The $LaNiO_3$ material was prepared by the modified proteic method, similar to that reported in the literature,[36,41] which consists of a modification of the protein sol-gel method.[51]

The preparation of the material by the modified proteic method was carried out using lanthanum nitrates (95.0%, Dynamic, São Paulo, Brazil) and nickel (97.0%, Vetec, Rio de Janeiro, Brazil) as starting material and collagen (NutriGold do Brasil, São Paulo, Brazil) as a complexing agent. The procedure for synthesizing the $LaNiO_3$ material consisted of dissolving 4.8767 g of nickel(II) nitrate in 100 mL of distilled water under magnetic stirring at 30 °C for 30 min. Then, 7.4055 g of lanthanum(III) nitrate were added to the system and kept under stirring for another

Table 3. Materials synthesized with perovskite structure and applied in the removal of dyes and experimental data

Material	Dye	Removal process	C / (mg L^{-1})	q / (mg g^{-1})	E_R / %	Reference
$LaNiO_3$	Reactive Black 5	catalytic oxidation	100	–	65	42
$CaTiO_3$	Methylene Blue	photocatalysis	10 20 30	–	89 79 55	43
$LaMnO_3$ $LaNiO_3$	Congo Red	adsorption	50	32 17	63 34	36
$CsPbI_3$	Methyl violet Rhodamine B Methyl Orange Acid Black 1 Malachite Green	photocatalysis	5	–	82 62 51 33 42	44
$LaFeO_3$	Rhodamine B	Fenton degradation	10	–	96	45
$ZnTiO_3$	Crystal Violet Rhodamine B	photocatalysis	10	–	93 95	46
$LaMnO_3$ $LaNiO_3$	Congo Red	adsorption	50	38 24	73 43	37
$LaAlO_3$	Direct Blue	adsorption	5	6	68	47
$LaFeO_3$	Rhodamine B	adsorption	100	182	99	48
$LaMnO_3$	Methylene Blue	adsorption	25	–	43	49
$BaBiO_3$	Rhodamine B	photocatalysis	5	–	80	50

C: solution concentration; E_R: efficiency removal; q: amount of dye adsorbed.

30 min. After this time, the solution was heated to 70 °C, when 4.8776 g of collagen were added. Thereafter, the temperature was maintained at 70 °C for 1 h, resulting in a viscous system that was heat treated at 350 °C for 2 h, with a heating rate of 10 °C min^{-1}. A precursor powder was obtained after the aforementioned heat treatment, which was separated into two parts: the first was calcined at 900 °C for 2 h at a rate of 10 °C min^{-1} and the rest was stored for future analysis. The precursor powder after the heat treatment was named LN-C35 and the sample calcined at 900 °C was called LN-C9.

Characterization of the synthesized material and dye

The powders obtained after synthesis and calcination and other materials obtained after the adsorption tests were characterized by physical-chemical techniques, including Fourier transform infrared spectroscopy (FTIR), X-ray diffractometry (XRD), scanning electron microscopy (SEM), adsorption of N_2 at 77 K, thermogravimetry analysis (TGA), determination of the pH of the zero charge point (pH_{PCZ}).

FTIR analyzes were recorded from 4000 to 400 cm^{-1} on a Varian 640-IR FT-IR spectrophotometer (California, USA), using the KBr method.

The X-ray diffraction patterns were obtained using Empyrean (PANalytical) X-ray diffractometer (Malvern, United Kingdom), operated with Cu Kα (λ = 1.5406 Å) and 2θ in the range of 10-65° and step size of 0.02° and a scanning speed of 0.5° min^{-1}. The XRD patterns were analyzed by Rietveld refinement.[52] The identification of the present phases was also carried out by comparison with the data from the ICSD (Inorganic Crystal Structure Database) and JCPDS (Joint Committee on Powder Diffraction Standards). From the X-ray diffraction pattern, the average crystallite size was calculated using the Scherrer equation.[53]

The obtained LN-C9 material was analyzed using scanning electron microscopy (SEM), HITACHI model TM 3000 (Tokyo, Japan).

The textural characteristic of the obtained LN-C9 material was determined by adsorption of N_2 at −196 °C in Quantachrome NOVA 1200 equipment (Florida, USA). The specific surface area was calculated using the Brunauer-Emmett-Teller (BET) method.

The pH of the zero charge point (pH_{PCZ}) was determined using the batch method equilibrium method, with initial pH values of 3, 5, 7, 9 and 11.

Thermogravimetric curves were obtained on a TA Q500 instrument (New Castle, USA) under an inert and dynamic atmosphere of nitrogen of 100 mL min^{-1}, in the temperature range of 30 to 900 °C, using approximately 5 mg of sample. Several researchers have proposed methods for obtain kinetic parameters starting from thermogravimetric data. The method proposed by Kissinger[54] uses the piecewise integration technique, where the kinetic parameters are changed by the variation of the maximum temperature peak (T_m) in relation to the heating rate (β), assuming that the reaction rate in a constant conversion depends only on temperature. Thus, the activation energy value is found by a simple linear regression. The activation energy value is obtained from slope of the graph of $\ln (\beta/T_m^2)$ *versus* $1/T_m$.

The study of the degradation of the dye (Turquoise Blue dye) and the mixture dye and perovskite (LN-C9) in the proportion 2:1 in mass was carried out. The FTIR spectra were obtained of the materials (dye and the mixture dye + perovskite) submitted to degradation at temperatures of 250, 500 and 750 °C, for a better understanding of dye decomposition.

Adsorption study with environmental contaminants

The absorbance spectrum of the Turquoise Blue dye solution and the analytical curve were obtained on an absorption spectrophotometer in the Shimadzu UV-1800 (Barueri, Brazil) UV-Vis region. For the absorption spectrum, the scan was applied in the wavelength range between 400 and 700 nm, whereas for the calibration curve, concentrations of 10, 20, 30, 40 and 50 mg L^{-1} were used, the study was carried out in triplicate.

For the adsorption studies was used the LN-C9 material previously dried at 60 °C for 30 min, aqueous dye solution at 30 mg L^{-1} and a temperature of 25 °C.

Initially, the optimization of the best adsorbate removal conditions was performed. The initial pH study was carried out using 50 mL of the synthetic effluent that underwent pH adjustments from 1.0 to 9.0, with the aid of solutions of 0.1 mol L^{-1} NaOH and 0.1 mol L^{-1} HCl. For each solution, 0.05 g of the adsorbent was inserted and the system was left under magnetic stirring for 30 min. After the pre-established time, the solid-liquid separation was performed and a supernatant portion was analyzed by UV-Vis spectroscopy for quantification.

In the study of the adsorbent mass, the values of 50, 100 and 150 mg were studied. A solution of the Turquoise Blue dye (250 mL) with pH adjusted for 3.0 was placed under stirring with LN-C9 adsorbent. After the pre-established time, an aliquot was removed, subjected to separation and the filtrate was analyzed by absorption spectrophotometry in the UV-Vis spectroscopy for quantification.

A study was also carried out to assess whether the aqueous solution of Turquoise Blue dye undergoes

photodegradation during the tests under the conditions used, but without the addition of the adsorbent. This evaluation was performed using 250 mL of the dye aqueous solution at pH 3.0 and no pH adjustment. At fixed time intervals, aliquots were collected, filtered and analyzed by absorption spectrophotometry in the UV-visible region.

After these optimizations, the study of the adsorption kinetics of the dye was performed using 250 mL of the aqueous solution of the Turquoise Blue dye at pH 3.0 with a concentration of 30 mg L^{-1} and 50 mg of the LN-C9 material (previously dried at 60 °C for 30 min), the study was carried out in triplicate, under magnetic stirring and at a temperature of 25 °C. At fixed intervals of 5, 15, 30, 60 and 90 min, aliquots were collected and filtered with the aid of filter paper to separate the adsorbent from the solution. For each aliquot, the filtrate was analyzed by absorption spectrophotometry in the UV-visible region, at a wavelength of 628 nm.[55]

For comparative purposes, tests were carried out with some adsorbent materials using the same conditions described above (solution volume = 250 mL; solution concentration = 30 mg L^{-1}; adsorbent mass = 50 mg (previously dried); under magnetic stirring and T = 25 °C) at pH 3.0 and without pH adjustment. After 90 min, aliquots were collected, filtrate and analyzed.

The values of removal efficiency (E) and the amount of adsorbed dye (q) in milligrams *per* gram of the adsorbent were calculated based on equations well disseminated in the literature.[55,56]

The kinetic models of pseudo first order (PFO), pseudo second order (PSO) and variable constants (VC) were used for the kinetic study of adsorption, as shown in equations 1, 2 and 3, respectively.[57,58]

$$q_t = q_e\left[1 - e^{(-k_1 t)}\right] \quad (1)$$

$$\frac{t}{q_{(t)}} = \frac{t}{q_e} + \frac{1}{k_2 q_e^2} \quad (2)$$

$$q_t = q_{AV}\left[1 - e^{(-k_{AV} t)^n}\right] \quad (3)$$

where q_t = adsorption capacity, q_e, q_{av} = maximum adsorption capacities, k_1, k_2 and k_{AV} = adsorption speed constants and n = adjustment parameter.

Study of the use in adsorbent cycles

The study of the use in cycles of the same adsorbent for the material LN-C9 was carried out in a batch system under agitation, temperature of 25 °C, 250 mL of an aqueous solution of the Turquoise Blue dye in a concentration of 30 mg L^{-1}, acidified to pH 3.0 and using 0.5 g of LN-C9 material (previously dried at 60 °C for 30 min). The system remained under constant agitation for 90 min and was subsequently subjected to filtration on filter paper. The resulting filtrate was dried in the oven at 60 °C for 30 min and then the remaining mass was applied again in a new solution of the dye with the same characteristics as the previous solution. This procedure was repeated for 6 consecutive times. In each test cycle, the filtrate was analyzed by absorption spectrophotometry in the UV-visible region, at a wavelength of 628 nm.

Recovery and reuse studies of the adsorbent

After the adsorption kinetics tests, the recovery process of the material used was carried out. The adsorbent/adsorbate system (retained in the filter paper) was dried in an oven at 60 ºC for 30 min, calcined at 900 °C for 2 h at a rate of 10 °C min^{-1} and then applied in a new test of adsorption with proportional reduction of volume of the dye solution and mass of the adsorbent. This calcination process was used to decompose the adsorbed dye. The adsorption test was carried out under the same conditions described in the adsorption kinetics and was carried out in order to assess whether the recovered material maintains its adsorption efficiency. The system containing the dye solution and the recovered adsorbent remained under constant magnetic stirring for 90 min, and was subsequently subjected to filtration on filter paper. The resulting filtrate was analyzed by absorption spectrophotometry in the UV-visible region, at a wavelength of 628 nm.

The materials recovered LN-C9/T (dry material after adsorption of the Turquoise Blue dye) and LN-C9/Tc (material calcined at 900 °C for 2 h after adsorption) were characterized by FTIR and XRD, in order to verify possible changes after adsorption, as well as to analyze if the initial structure of the adsorbent is maintained after calcination of the material resulting from the adsorption.

Results and Discussion

Synthesis of $LaNiO_3$ material

The FTIR spectra shown in Figure 1 are of the $LaNiO_3$ material synthesized by the modified proteic method and of the collagen. The analyzed samples were collagen, precursor powder (LN-C35) and material calcined at 900 °C (LN-C9).

The FTIR spectrum of collagen shows the main characteristic bands at 1650 cm^{-1}, typical of amide I, due to the stretching of the carbonyl;[59] in 1539 cm^{-1}, related to

amide II, due to vibrations in the plane of the N–H bond and the C–N stretch;[60] in 1240 cm^{-1}, they correspond to the vibrations in the amide III plane, due to the C–N stretch and the N–H deformation; at 1450 cm^{-1}, corresponding to the stereochemistry of the pyrrolidine rings.[61]

In the spectrum of the precursor powder LN-C35, a wide band at 1463 cm^{-1} can be observed, characteristic of the overlapping of the bands attributed to the stretches of the carboxylic and amino groups of the complexing agent. It is observed that this band appears displaced to smaller wave numbers, which probably occur because of the coordination of the metal cations with the amino and carboxylate groups belonging to the complexing agent. In the 895-820 cm^{1} range, two bands appeared which, according to the literature, can be attributed to the possible coordination of the carboxylate groups with the metals present.[60]

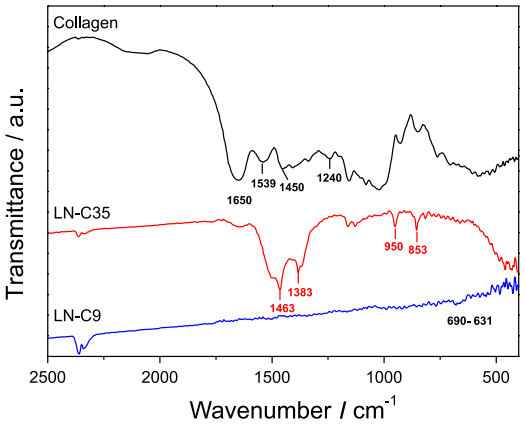

Figure 1. FTIR spectra for collagen, LN-C35 and LN-C9 materials.

The FTIR spectrum of the LN-C9 material did not show the bands seen in the spectrum of the LN-C35 material. The disappearance of these bands is suggestive that carboxylic and amino groups of the collagen were coordinated to the ions metallics. Bands observed in the 686-640 cm^{-1} range can be attributed to the metal-oxygen bond, evidencing the idea of formation of the mixed perovskite oxide, in which the metals are coordinated with the oxygen atoms.[41]

The confirmation of the oxide phase formed was obtained through the X-ray diffraction pattern of the LN-C9 sample. Figure 2 shows the X-ray diffraction pattern for the synthesized and calcined material at 900 ºC. The analysis of the patterns using the Rietveld refinement indicate that $LaNiO_3$ with perovskite structure and rhombohedral geometry was formed, with a space group *R-3c*. The lattice parameters, volume and phase percentage for the $LaNiO_3$ extracted from the Rietveld refinement results were: a = b = 5.482655 Å and c = 13.306940 Å; volume (Å^3) = 346.410 and 93.2%, respectively. As the calculated value of the $LaNiO_3$ phase percentage is of 93.2%, this indicates that secondary phases are in low amounts.

The observed diffractogram showed a high intensity peak of 2θ at 32.71º and others, less intense peaks, at 23.10, 40.48, 47.19, 53.36 and 58.41º, that were indexed and also confirmed the formation of the perovskite structure with rhombohedral geometry, according to letter JCPDS 33-0711. The LN-C9 material also showed some low intensity peaks due to secondary phases, with peaks in: 2θ = 28.51 and 29.80°, which according to ICSD letter No. 25-7585 refers to lanthanum oxide (La_2O_3), while the peaks 2θ at 37.14 and 43.20º, according to ICSD letter No. 25-9699 are associated with nickel(II) oxide (NiO).

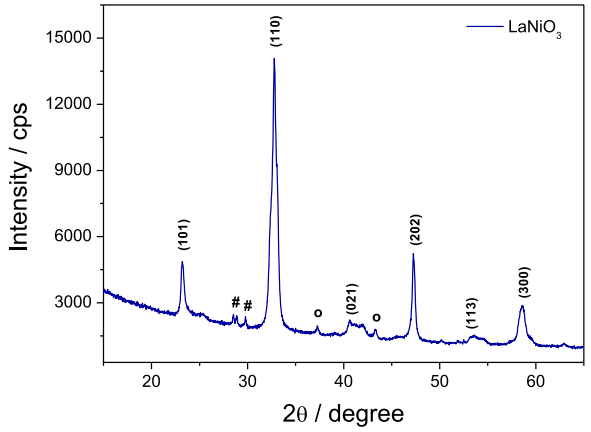

Figure 2. X-ray diffractogram of the $LaNiO_3$ material. Where: La_2O_3 (#) and NiO (°).

Through the diffraction peaks of the synthesized material, it was possible to calculate the average crystallite size, with a value of 19 nm. A similar value was previously reported for perovskite $LaNiO_3$ synthesized by the modified protein method using soy protein as a chelating agent.[36]

Through the diffraction peaks it was also possible to identify the type of crystalline structure of the studied material. Note the presence of a rhombohedral geometry, which is quite common for this type of material, as shown in Table 2. Still according to the data in this table, it can be inferred that the size of the crystallite of the material synthesized in this work is larger when compared to materials with the same structure synthesized by the mechanosynthesis method and lower when the synthesis method is hydrothermal.[40,62]

The size of the crystallite directly influences the specific surface area, where the smaller the crystallite size, the greater the value of the surface area. For this work, the value of the surface area of the LN-C9 sample was 22 $m^2 g^{-1}$, presenting a similar way to those reported in the literature, where the values of 26 and 25 $m^2 g^{-1}$ were

obtained for the material with $LaNiO_3$ structure, calcinated at 700 °C by the modified protein method using soy fiber and collagen, respectively.[41,63] It is noted that the value of the obtained surface area is similar to that of materials with this type of structure when synthesized by the same method citric acid sol-gel.[30,34] In general, the surface areas of perovskites are low, as the synthesis methods involve very high temperatures in calcination.

Working with collagen in powder form increases the contact surface between the reagents, thus, a greater volume of organic matter is impregnated in the structure and during calcination, the organic matter is eliminated, providing the formation of cavities, which can contribute to the development of pores. Scanning electron microscopy (SEM) was used to visualize the morphology of the synthesized material. Figure 3 shows the presence of fine and porous particles, uniformly agglomerated with different pore sizes.

Figure 3 shows a homogeneous surface, this may be associated with the fact that collagen supplies the system with a large amount of organic matter, which is eliminated during calcination, favoring the appearance of pores in the material.[64]

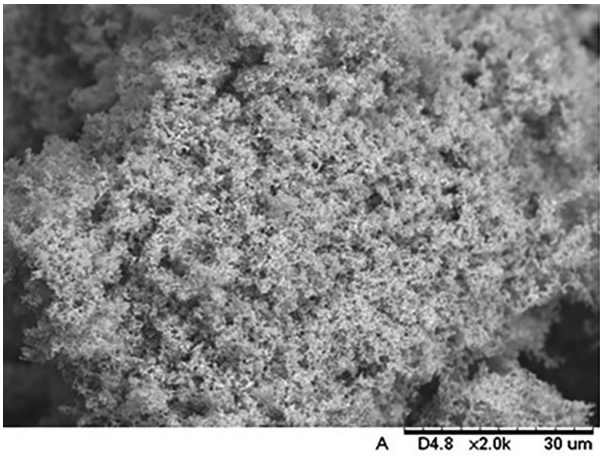

Figure 3. SEM of the $LaNiO_3$ material (LN-C9).

The adsorptive processes depend on some factors, among them are the pH of the solution and the affinity of the adsorbent with the adsorbate. The surface charges of the adsorbent, which depend on the pH, can be manipulated with acidic or basic treatments. It is worth mentioning that the knowledge of surface loads is essential to know the best pH for a greater retention of the residue on the material surface.

The pH of the zero charge point (pH_{PCZ}) is the point at which the pH of the material surface is neutral (zero charge). The determination of the pH_{PCZ} is very important to know the behavior of the material according to the amount of (H^+) and (OH^-) present in the solution. The LN-C9 material has a zero charge point (pH_{PCZ}) equal to 7.44 (Figure S1, Supplementary Information (SI) section), this value is consistent with data from the literature that presents pH_{PCZ} in the range of 6.22 to 9.2 with lanthanum at site A of perovskite structure.[62]

Given the zero charge point value, it can be said that if the pH of the solution is above pH_{PCZ}, the surface of the material will be negatively charged and it will have greater affinity in adsorbing cations. On the other hand, if the pH of the reaction medium is below the pH_{PCZ} of the material, the surface will be positively charged and it will tend to adsorb anions. Thus, as the Turquoise Blue dye is an anionic dye, the pH of the dye solution must be lower than pH_{PCZ}, so that the affinity between the adsorbent and the adsorbate is maximized and, consequently, the removal efficiency is greater.

Studies for removal of Turquoise Blue dye

Characterization of solid and solution Turquoise Blue dye

Figure 4a shows the FTIR spectrum of the Turquoise Blue dye. In this spectrum, a broadband in the region of 3656-3171 cm^{-1} is observed, referring to the stretching of the O–H water connection, probably due to the humidity present in the sample. Absorption of stretches of the C=C bond of the aromatic ring were observed as a doublet at 1635 and 1595 cm^{-1} and, at 1227 cm^{-1}, a characteristic stretch of the C–N bond is observed.[40,65] At 1136 cm^{-1} there is an intense band referring to the stretching of the connection –C–N=. The bands whose wavelengths are 617, 681, 744, 833 and 1027 cm^{-1} can be associated with stretches of the S–O bond.[65]

Looking at Figure 4a, it can be seen that the bands shown are in accordance with the connections present in the dye structure. It is noteworthy that the band at 1136 cm^{-1} referring to the stretching of the connection it is probably related to the bonds of the dye chromophore group, copper phthalocyanine. Among the groups present in the structure of the Turquoise Blue dye, electronic density donor groups such as $(SO_3)^-$, whose coordination points are oxygen and groups (NH_2), in which the coordination points are nitrogen atoms, are identified as possible adsorption sites.[40]

In order to evaluate the thermal stability of the solid Turquoise Blue dye, a study of the variation of mass as a function of temperature was carried out. Figure 5a shows thermogravimetry/derivative thermogravimetry (TG/DTG) curves for the dye obtained at different heating rates and Table 4 shows the theoretical and experimental values of mass losses and respectively temperature range.

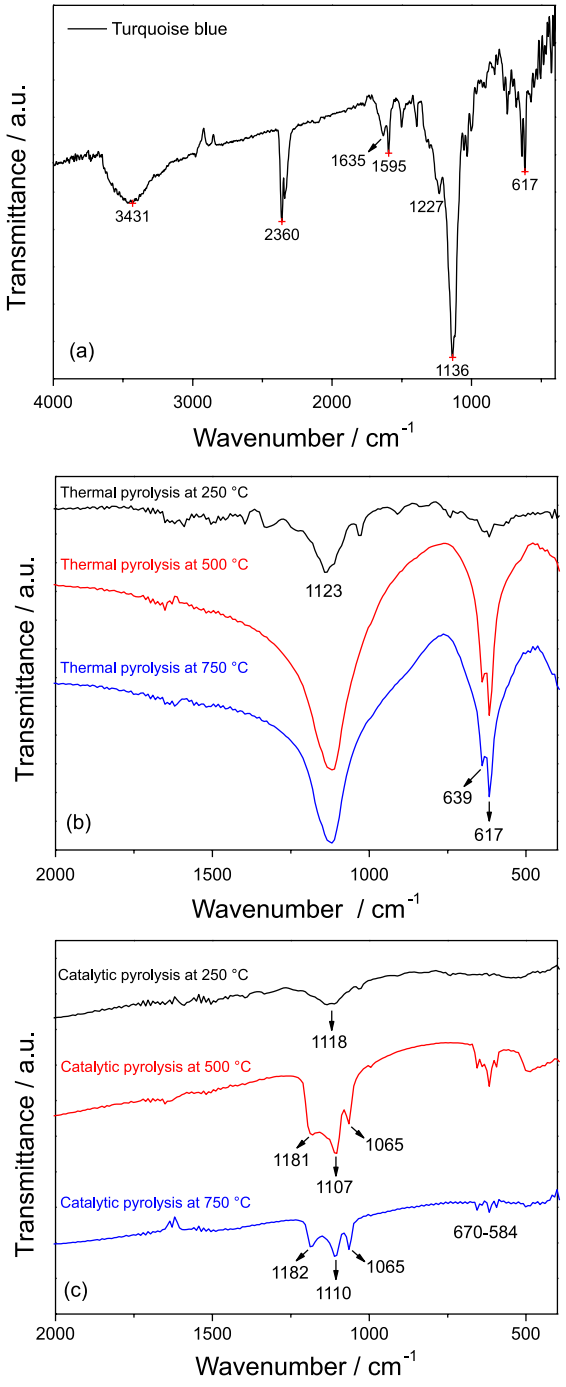

Figure 4. FTIR (KBr) spectra of the Turquoise Blue dye: (a) solid, (b) at different thermal pyrolysis temperatures and (c) at different catalytic pyrolysis temperatures using LN-C9.

All TG/DTG curves showed an initial mass loss in the range of 25 and 200 °C due dehydration. The thermal pyrolysis of the dye occurs in two major decomposition events in the range of 155 and 900 °C and all organic material from the dye is not decomposed at 900 °C. These events are associated with a part of the dye structure decomposition. The events that occur in the temperature range of 155 at 900 °C correspond to mass losses of about 56-69% and are attributed to the decomposition and oxidation of organic matter from the dye and also probably due to the thermal decomposition of Na_2SO_4, obtaining about 26-40% of residue, probably from sodium oxide and copper compound, named from CuZ and CuX, where Z contain four nitrogen, four carbons and four hydrogens and X is the fragment of dye that contain four compounds with theorical formula C_4H_6N.

The temperature required for dye decomposition via thermal pyrolysis is affected by the heating rate; and as well as the composition of the final residue. When the analysis is done at 5 °C min^{-1}, 69% of the dye is decomposed until 900 °C and the percentual of final residue (26%) is different from when the analyzes are done at 10 or 20 °C min^{-1}, where final residues (at 900 °C) are about 40%, and only about 56.5% of the dye is decomposed. The results indicated that the system is mainly affected by the heat transfer limitations, and with the increase of the heating rate an increase of the event temperature occurs due to a less efficient heat transfer. From TG/DTG data it was also determined the purity of the dye, since we have the theoretical and experimental values, and the dye studied is 96% pure.

Table 5 shows the kinetic data for the main events of the dye decomposition. It can be observed a decrease in activation energy with increasing T_m, indicating that a progressive increase in the maximum reaction rate temperatures leads to less energy expenditure in the process.

Figure 4b shows the FTIR spectra of the Turquoise Blue dye submitted at different thermal pyrolysis temperatures (250, 500 and 750 °C). When analyzing the spectra of the materials obtained from the dye pyrolysis at different temperatures, the presence of a broad and strong band in the region of 1123 cm^{-1} is noted, referring to the asymmetric stretching of the (SO_4^{2-}) groups. Bands in the region of 639 and 617 cm^{-1} were observed for all materials, which may be associated with the asymmetric flexion of the (SO_4^{2-}) groups and with the stretches of the S–O bond, effect of the decomposition of organic matter and the possible formation of sodium compounds.

The calibration curve of the aqueous solution of the Turquoise Blue dye with and without pH correction to the value 3.0 was obtained in order to determine the actual concentration of the dye used in the experiments of this work, this was possible through the linear equation obtained, as shown in Figure S2 (SI section). It is worth mentioning that the reading of the aqueous solution was performed at 628 nm. When analyzing Figure S2, it can be seen that both curves presented satisfactory correlation coefficients (R^2), and the curve with pH measurement showed the R^2 closest to 1.

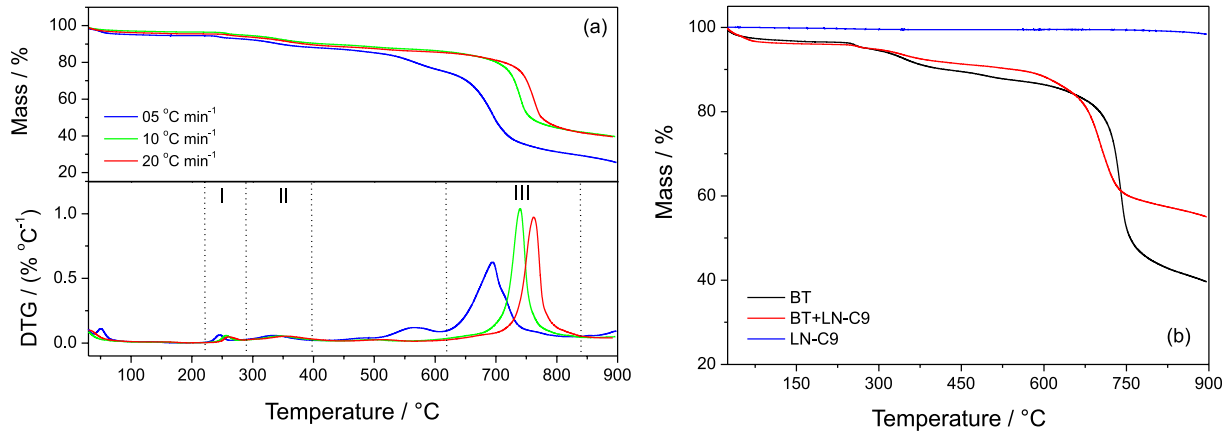

Figure 5. (a) TG/DTG curves of the Turquoise Blue dye at different heating rates and (b) TG curves of the Turquoise Blue dye (BT), $LaNiO_3$ (LN-C9) and mixture of BT + LN-C9 materials.

Table 4. Data from the thermal analysis of the Turquoise Blue dye at different heating rate and from the thermal analysis of the mixture dye + LN-C9 obtained at 10 °C min^{-1} heating rate

Heating rate / (°C min^{-1})	Temperature range / °C	Experimental mass / %	Theoretical mass / %	Assignment
Data from TG/DTG curves of the Turquoise Blue dye				
	25-155	5.4	5.4	$4H_2O$
5	155-900	69.0	69.8	CHSO
	900	25.7	24.8	$2(Na_2O_2)$, CuZ
	25-172	3.5	2.8	$2H_2O$
10	172-900	57.1	60.2	CHSO
	900	39.6	37.0	$2(Na_2O_2)$, CuX
	25-196	4.5	4.1	$3H_2O$
20	196-900	55.9	59.4	CHSO
	900	39.6	36.5	$2(Na_2O_2)$, CuX
Data from TG/DTG curves of the mixture of Turquoise Blue dye and LN-C9 material				
	25-200	4.1	3.5	$3H_2O$
10	200-900	40.9	43.8	CHSO
	900	55.0	52.7	$2(Na_2O_2)$, CuJ, $LaNiO_3$ and sulfate

CHSO: organic matter and sulfate; CuX, CuZ and CuJ: residual compounds.

Table 5. Maximum reaction rates temperatures (T_m) as a function of heating rate for decomposition of the dye

Heating rate / (°C min^{-1})	Event I	Event II	Event III
5	246.8	336.0	695.4
10	258.1	344.8	740.6
20	261.9	358.7	763.2
Eat / (kJ mol^{-1})	186.93	182.98	146.63

Eat: activation energy.

In order to better understand the behavior of the Turquoise Blue dye with and without pH measurement, the UV-Vis spectra were obtained (Figure S3, SI section) and it was observed that with the addition of 0.1 mol L^{-1} HCl to acidify the solution, it was verified a change of one of the absorption bands characteristic of the chromophor groups that gives the color, indicating a possible change in the structure of the dye. Another factor that helped this investigation was the color change observed in the solution of the Turquoise Blue dye when there was a pH reduction, changing from blue to green (insert in Figure S3).

The Turquoise Blue dye is a reactive dye and its chromophore group consists of copper phthalocyanine. Blue copper phthalocyanine is a Cu^{II} complex and the elevation of the ring's degree of halogenation gradually transforms the natural bluish color of phthalocyanine to greenish tones, generating phthalocyanine greens. This fact can be confirmed according to insert in Figure S3 (SI section), which shows the color change of the solution from blue to a more greenish tone when HCl is added to change the pH.

Solar radiation is essential for ecosystem processes, directly influencing photosynthesis, as well as the degradation of organic materials. Thus, considering the possibility of degradation of dyes under the presence of visible light, a study was carried out to assess whether the Turquoise Dye can be photodegraded during the adsorption experiments and under visible light. The study to assess whether photodegradation of the Turquoise Blue dye solution occurs was carried out without the addition of adsorbent material, under the action of visible light, with and without measuring the pH of the medium for 90 min, and the results can be seen in Figure 6.

After the dye photodegradation evaluation tests with and without pH measurement, it was observed that the dye does not decrease the initial absorbance with the effect of visible light during the time of the experiments.

Studies using $LaNiO_3$ material

The influence of pH on the adsorption of dyes indicates that there is a balance between ionic species and the interactions of the system are influenced by the change in the pH of the medium. The influence of the initial pH of the Turquoise Blue dye solution on the adsorption by the synthesized perovskite is shown in Figure 7a through the values of the dye removal efficiency, E (%).

The synthesized material ($LaNiO_3$) showed greater removal of the dye at pH 3.0, suggesting that the main interaction involved is the electrostatic interaction, since at the natural pH of the aqueous solution of the dye that is equal to 6.0 the adsorption is low, as also observed by other works.[11]

It is observed that the synthesized material showed better removal of the dye at acid pH values. These values are consistent with works in the literature that studied the removal of the Turquoise Blue dye, finding pH 1.0 as the best pH using zeolite as an adsorbent and pH 2.0 using commercial activated carbon.[11,12] In addition, the values obtained from the zero charge point indicate better removal of anionic dyes at pH values below the zero charge point, since at pH values lower than pH_{PCZ} the material surface

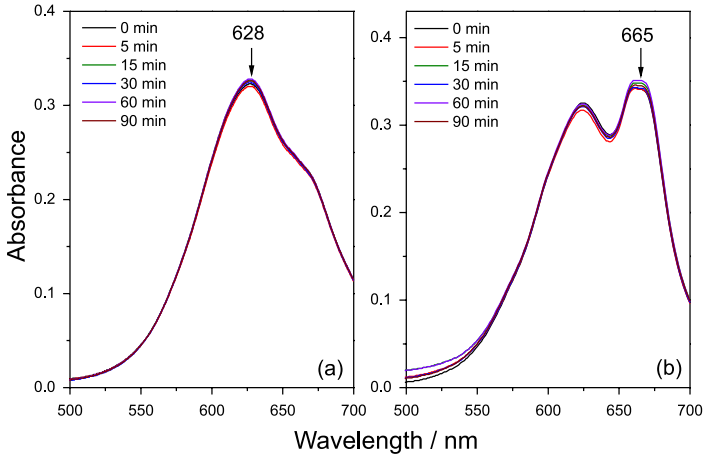

Figure 6. Evaluation of the photo-degradation of the Turquoise Blue dye with pH correction (a) and without pH correction (b) as a function of time.

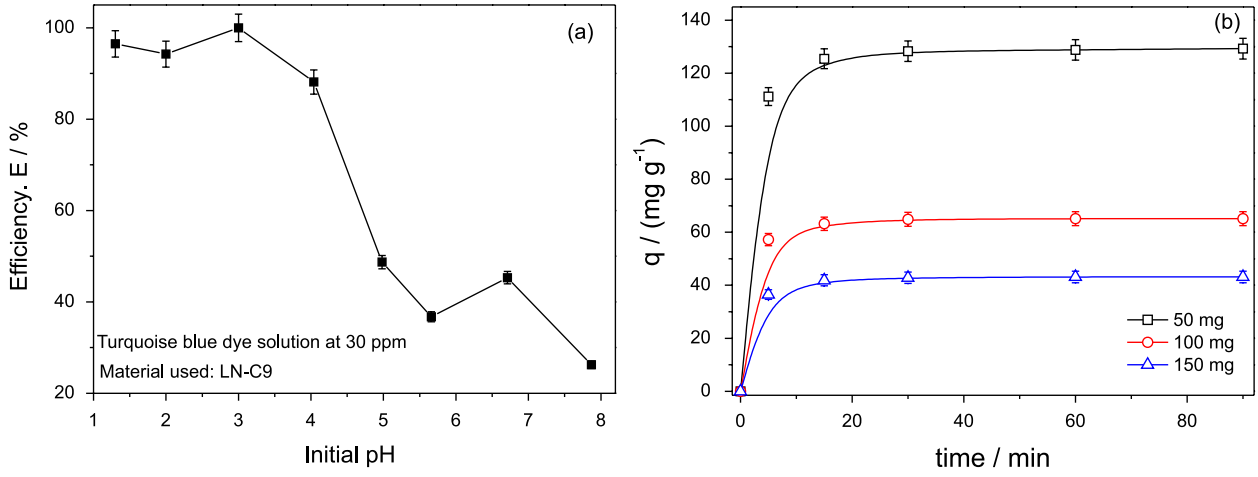

Figure 7. Efficiency of removal of the Turquoise Blue dye as a function of the initial pH (a) and amount of Turquoise Blue dye removed by mass of adsorbent at pH 3.0 (b).

will be positively charged and the particle will tend to adsorb anions. Thus, at acid pH (lower than pH_{PCZ}) the interaction between adsorbent and adsorbate is greater since the Turquoise Blue dye has sulfonate groups, responsible for its anionic character, therefore having a negative surface charge.

In addition to knowing the influence of the pH of the reaction medium on the adsorption process, it is also necessary to understand how the mass of the adsorbent can interfere in this procedure, in order to optimize the best experimental conditions. The influence of the adsorbent mass is expressed in Figure 7b. It is noteworthy that this study was carried out with the material synthesized in contact with the dye solution at pH 3.0.

According to Figure 7b, it is noted that the 50 mg mass was the one that presented the best result. This fact was expected since the amount of adsorbed dye is inversely proportional to the mass of adsorbent used.[55] It is worth mentioning that for both mass values the removal efficiency was practically the same, around 90%, suggesting that after a certain amount of mass, the balance between the liquid and solid phases is obtained, that is, there will be no further removal of the compound even if the amount of the adsorbent is increased. Possibly if the mass of the adsorbent were reduced, there would be less removal of the dye.

The adsorption performance can be expressed by the adsorption efficiency, E(%) and the amount of adsorbed dye (q). With regard to efficiency, it becomes greater as there is a mass transfer of the dye solution to the adsorbent material, thus decreasing its concentration.

The synthesized and calcined material ($LaNiO_3$) was applied in adsorption tests in order to verify the ability to adsorb the Turquoise Blue dye from the aqueous medium. Figure 8 shows the adsorption efficiency and the amount of Turquoise Blue dye adsorbed (q) on the LN-C9 material at different times. It was observed that over time, the concentration of dye in the solution decreases and consequently the values of the adsorption efficiency (E) increase.[40]

It is observed that the values increase rapidly in the first 5 min of contact between the adsorbent and the Turquoise Blue dye and start the stabilization around 15 min and remain constant in 30 min until the end of the experiment with maximum values of E% and q of approximately 88% and 131 mg g^{-1}, respectively.

As can be seen in Figure 8, the adsorption equilibrium is reached in 30 min, since no additional adsorption is observed with the continuity of time. This is due to the high affinity between the surface of the adsorbent with groups or molecules of the dye, the mass transfer of the

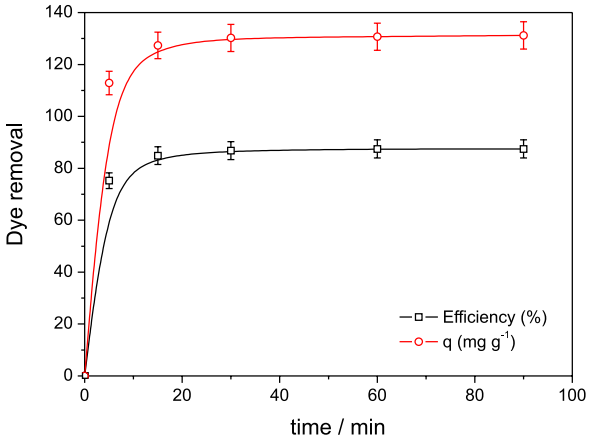

Figure 8. Removal efficiency and amount of adsorbed Turquoise Blue dye (q) when used the LN-C9 adsorbent, at pH 3.0, at 25 °C, at a concentration of 30 mg L^{-1}.

solution of the dye to the adsorbent reaches equilibrium in that time interval.[66]

In adsorption processes, the adsorbent molecules can fragment, losing their original structure, dividing into radicals which are attached to the surface of the adsorbent. One can then consider a possible coordination between the cations of the B site of perovskite with donors groups of electronic density present in the structure of the Turquoise Blue dye such as (SO_3^-), whose coordination points are oxygen, in addition to the groups (NH_2) and (N=N), where the coordination points are the nitrogen atoms.[40]

The kinetic study was performed using the models of pseudo first order (PFO), pseudo second order (PSO) and the variable constants. Table 6 shows the results of study of adsorption kinetics using three models for the LN-C9 material. In addition, Table 6 shows the amounts of dye adsorbed in the equilibrium, the speed constants, the correlation coefficients, χ^2 and standard deviation of each model.

Analyzing the results, it can be seen that the three models applied are very similar to the experimental data, presenting close amounts of the adsorbed dye, but due to this similarity, these data are insufficient to indicate which model is more suitable for assessing the adsorption kinetics.

The three kinetic models presented high values of linear coefficients, indicating the effectiveness of the application of the models for the studies of the tests. However, the kinetic model of the variable constants presented a higher value of the correlation factor, quantities of dyes closer to the experimental values, as well as lower values of χ^2 and standard deviation.[67]

Lagergren's first order equation suggests that adsorption has its mechanism controlled by diffusion, considering that adsorption occurs due to the difference in concentration between the surface of the adsorbent and the solution.

Table 6. Parameters obtained by the pseudo first order, pseudo second order and variable constants for the adsorption kinetics of the Turquoise Blue dye under the LN-C9 material

Pseudo first order					
k_1 / min^{-1}	q_1 / (mg g^{-1})		R^2	χ^2	SD
0.4041 ± 0.0177	129.4508 ± 0.6949		0.99944	0.1608	0.0191
Pseudo second order					
k_2 / (g mg^{-1} min^{-1})	q_2 / (mg g^{-1})		R^2	χ^2	SD
0.0086 ± 0.0007	132.7751 ± 0.6390		0.99972	0.0325	0.0081
Variable constants					
k_{AV} / min^{-1}	q_{AV} / (mg g^{-1})	n	R^2	χ^2	SD
0.7113 ± 0.0251	130.4692 ± 0.1204	0.5375 ± 0.0144	0.99999	0.0280	0.0078

q_1, q_2, q_{av}: maximum adsorption capacities; k_1, k_2 and k_{AV}: adsorption speed constants; n: adjustment parameter; R^2: correlation coefficients; χ^2: chi-square; SD: standard deviation.

The second order equation shows that adsorption involves sharing and exchanging electrons, that is, there is chemisorption. The equation of the variable constants describes reactions of fractional orders, suggesting that the interaction processes undergo changes in the reaction mechanism and speed during the analyzed time.[67,68]

It is possible to verify that the experimental data are better suited to the kinetic model of variable constants. This result can be confirmed by observing the correlation factors R^2, χ^2 and SD (Table 6). In this way, it can be seen that the correlation factors are closer to 1 for the model of variable constants, therefore, it is considered that this model fits better to the studied adsorption. It is assumed that the interaction between the dye and the adsorbent material occurs due to a high electrostatic attraction between the positively charged surface of the adsorbent, due to the cations and the negatively charged surface of the Turquoise Blue dye, acquired by the presence of the sulfonate groups.

In order to try to understand the interaction of the $LaNiO_3$ adsorbent with the Turquoise Blue dye, tests were performed under the same conditions for comparative purposes with other materials and the results are shown in Table 7.

The results indicate that when the pH of the dye solution is adjusted to 3.0, occurs an improved removal efficiency of dye when used all studied adsorbent materials. This fact may be associated with electrostatic interactions between the dye charges and of the analyzed materials, since the values of the charge point zero of the studied materials indicate better anionic dye removal at lower pH values than pH_{PCZ}, and similar results was also observed.

When comparing the materials synthesized in this work with the silicas, it is noticed that there is a greater removal efficiency for the $LaNiO_3$ materials with perovskite structure, this probably occurs because of the supposed interaction between the coordination points of the dye with the metals that occupy the B site of perovskite, since the studied silicas do not contain metals in their composition.

When analyzing the oxides used as starting material for the synthesis in the removal of the Turquoise Blue dye, it is noted that they present a good removal efficiency both with and without pH measurement. For results without pH measurement this was expected, since the pH_{PCZ} of these materials are higher than that of the material synthesized in this work, suggesting that in the natural pH of the dye (pH 6.0) there is already a good interaction between the dye and the adsorbent. With the pH measurement, the

Table 7. Removal efficiency (E) and amount of adsorbed dye (q) for $LaNiO_3$ (LN-C9) material and other materials with and without pH adjustment

Material	pH_{PCZ}	Without pH adjustment		With pH adjustment	
		E / %	q / (mg g^{-1})	E / %	q / (mg g^{-1})
LN-C9	7.4	36	53.7	88	131.2
Silica gel	6.6	0.5	0.8	49	73.2
Fummed silica	5.5	0.3	0.4	51	76.7
La_2O_3	9.0	57	85.6	88	132.0
Ni_2O_3	10.6	70	104.9	87	131.0
Activated carbon	8.3	85	127.3	91	136.2

pH_{PCZ}: pH of the zero charge point; E: removal efficiency; q: amount of adsorbed dye.

results are similar to that of the $LaNiO_3$ material with a perovskite structure, however the use of mixed oxides is able to reduce the cost of the adsorbent material and generate a material less impacting to the environment.

Observing the results of removing the Turquoise Blue dye when commercial activated carbon is used as an adsorbent, it can be noted that the values of E and q are the largest. Among the factors that may have contributed to this better efficiency, there may be a greater surface area and the presence of surface groups that improve the interaction with the dye groups. However, the inefficiencies in some types of dyes and the high cost in the processes of acquisition, operation and regeneration make the use of activated carbon unviable, mainly in countries with low financial conditions.[69]

Based on Table 7, the material synthesized in this work has removal efficiency and/or favorable amount of adsorbed dye when compared to works in the literature that use the Turquoise Blue dye as adsorbate under conditions similar to this work. It is also worth mentioning that in all the works mentioned in Table 1, the pH influences a lot in the adsorption, being the acid medium favorable.

Figure 9 shows the possible interaction between the Turquoise Blue dye and the $LaNiO_3$ material with a perovskite structure. It is observed that the adsorption process is governed by electrostatic interactions between anionic groups of the dye and the metals of the B site of perovskite.

Analyzing Figure 9, it is possible to confirm the anionic nature of the dye through the sulfonic groups (SO_3^-), which are responsible for interacting with the metals La^{3+} and Ni^{3+} that are present in the perovskite structure. In addition, the influence of the measurement of pH = 3.0 is highlighted, which is lower than pH_{PCZ} favoring a greater electrostatic interaction between the dye and the adsorbent.

At the end of the adsorption process, it is necessary to provide a suitable destination for the material formed, which is composed of the adsorbent/adsorbate system. Thus, it is proposed that such a system be subjected to calcination, in order to promote the decomposition of organic matter, which comes from the dye (adsorbate). In view of the above, the adsorbent/adsorvate system was submitted to FTIR and XRD analysis, to analyze the possible groups present and if the adsorbent structure is maintained. The LN-C9/T material was subjected to analysis, which comes from the LN-C9 sample after adsorption of the Turquoise Blue dye and dried at 60 °C for 30 min. In addition, the characterization of the calcined material was carried out after adsorption (LN-C9/Tc) at 900 °C for 2 h to verify whether it maintained its initial structure.

To prove that the perovskite structure was maintained after the adsorption tests and subsequent recovery, XRD analyzes were performed for the samples obtained. The diffractogram is shown in Figure 10a and shows the peaks for the perovskite phase with 2θ at 23.21; 32.82; 40.56; 47.28; 53.42 58.62º, according to JCPDS standard No. 33-0711, with rhombohedral geometry.

Note that the materials after adsorption (LN-C9/T) and calcined after adsorption (LN-C9/Tc) maintained the peaks of $LaNiO_3$ perovskite, indicating that the structure was not compromised with the process and that it can be used again.

Figure 10b shows the FTIR spectra of the samples before the adsorption test, after the adsorption test and dried at 60 °C for 30 min, and calcined at 900 °C for 2 h after the adsorption test, such spectra will be compared with that of pure dye (Figure 4a).

In the spectrum of the dry material after adsorption (LN-C9/T) there is the appearance of bands in the region from 1755 to 1475 cm^{-1} corresponding to the stretching of the aromatic ring C=C bond, suggesting that there was adsorption of the Turquoise Blue dye in the $LaNiO_3$ material with perovskite structure, since these bands are characteristic of groups present in the dye. When analyzing the spectrum of the calcined material after adsorption,

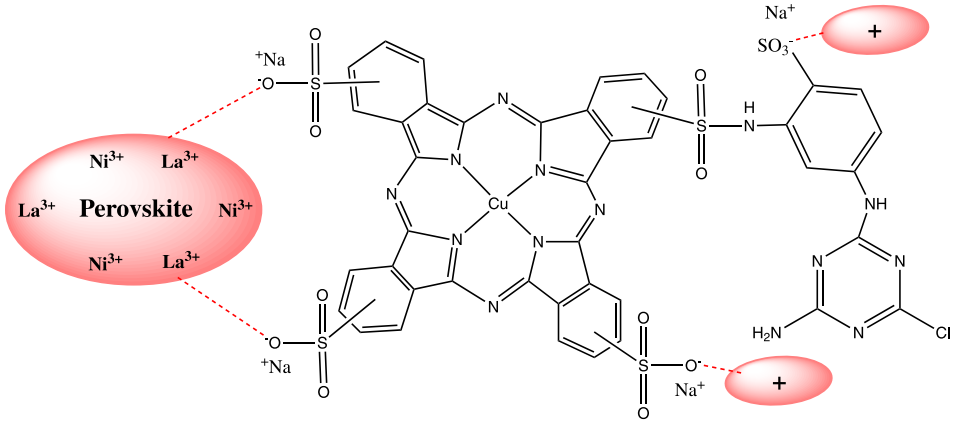

Figure 9. Interaction model proposed between the Turquoise Blue dye and the $LaNiO_3$ material with perovskite structure.

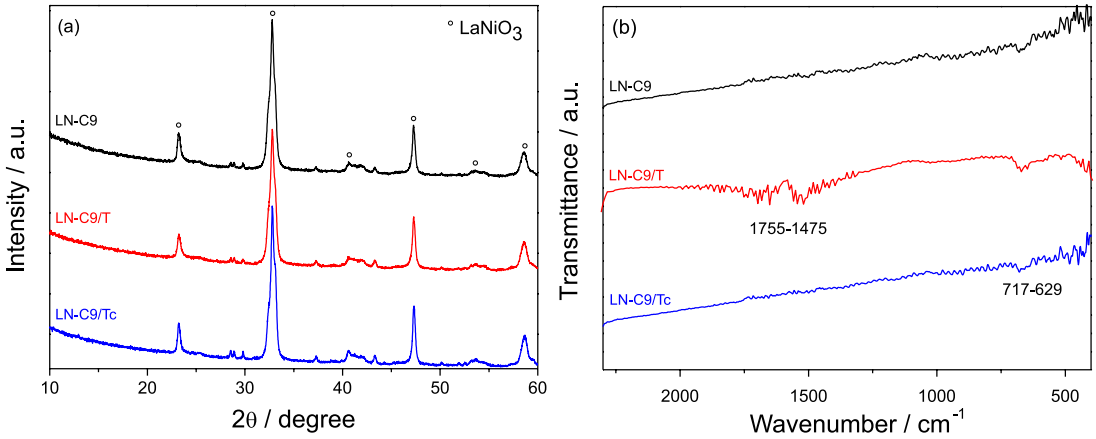

Figure 10. X-ray diffraction pattern (a) and FTIR spectra (b) of the material $LaNiO_3$ before (LN-C9), dried after adsorption with the Turquoise Blue dye (LN-C9/T) and after calcination (LN-C9/Tc).

the efficiency of the calcination is perceived, since the characteristic groups of the dye practically do not appear, indicating that there was a decomposition of the organic groups.

The other bands that are in the region between 717 and 629 cm^{-1} for all materials are evidence that the perovskite structure was not destroyed, as they are attributed to the stretching of the metal-oxygen bonds.[41]

When comparing the spectra of LN-C9 and LN-C9/Tc material, it can be seen that the structures appear to be practically the same, suggesting that the calcination temperature used to degrade the impregnated dye was efficient. Thus, it is assumed that the material obtained at the end of the calcination is the recovered perovskite, which can be tested in other adsorption tests.

In order to evaluate the useful life of the adsorbent in the removal of the Turquoise Blue dye, the LN-C9 material was used in cycles without calcination after analysis. With this study it was possible to notice that the same material was able to be used 6 times while maintaining an excellent removal efficiency, as shown in the data in Figure 11.

In Figure 11, it is noted that the studied material can be used efficiently in adsorption in cycles of the Turquoise Blue dye with efficiencies greater than 90% for all cycles.

A similar study of the literature using rice husk ash as an adsorbent was carried out in continuous reuse cycles in a residual textile dyeing bath containing the dyes Yellow remazol ultra RBG and Red remazol RGB gran, where the 5 cycles performed decreased their removal efficiencies to approximately 46% in the last cycle.[70]

When comparing the study mentioned above with the one carried out in this work, it is noted that the efficiency of removal of the studied material ($LaNiO_3$) practically does not lose its efficiency throughout the cycles, reaching 91% in its 6th cycle, which can promise the use of these as adsorbent materials in the removal of dyes.

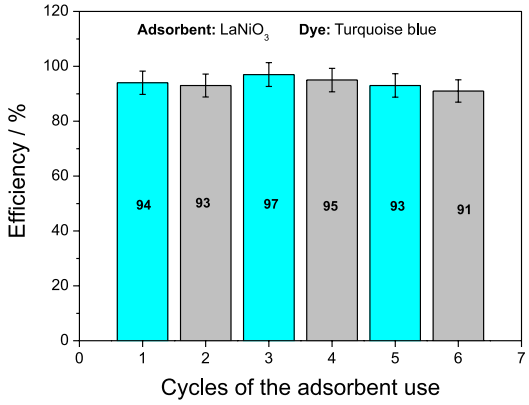

Figure 11. Efficiency of removing the Turquoise Blue dye by the LN-C9 material in cycles.

Figure 5b shows TG curves for Turquoise Blue dye (TB), LN-C9 material and for the mixture composed of dye and LN-C9 (TB + LN-C9) material obtained at 10 °C min^{-1} of heating rate and Table 4 shows the theoretical and experimental values of mass losses for the analysis of TG curves. The LN-C9 material showed thermal stability throughout the temperature range studied and no mass loss was observed. For the mixture it is possible to observe the first loss of mass referring to water in the temperature range of 25 to 200 °C, which corresponds to the loss of 4.1%. The events that occur in the temperature range from 200 to 900 °C correspond to mass losses of 40.9% and are attributed to the decomposition and oxidation of organic matter (from dye), and also probably due to the partial decomposition of Na_2SO_4.

Although all organic material from the dye is not decomposed at 900 °C, the temperature of the main dye decomposition event (T_m = 741 °C for pure dye) is lowered when LN-C9 material is mixed with the dye (T_m = 703 °C for dye in the mixture). The results suggests that the interaction with the adsorbent causes the dye to decompose faster, the material being a possible catalyst for

the dye decomposition reaction. For the other side, the final residue at 900 °C of the Figure 5b contains a slightly higher percentage of dye decomposition residues when compared to pure dye decomposition (Figure 5a and Table 4), which suggests a different mechanism for dye decomposition when it is mixed with the $LaNiO_3$.

As $LaNiO_3$ oxide is a thermally stable material throughout the temperature range studied, it is kept together with the final residue at 900 °C, which is also probably composed of sodium oxide, sulfate and copper compound, named CuJ, where J contain four nitrogens, sixteen carbons and eight hydrogens, that are fragments from dye decomposition.

FTIR spectra were also obtained for these samples (mixture of the LN-C9 and dye at different temperatures). Figure 4c shows the FTIR spectra of the LN-C9 + dye as a function of temperature subjected to degradation at temperatures of 250, 500 and 750 °C.

When the spectra of Figure 4c are evaluated, the presence of bands in the region of 1181-1065 cm^{-1} is noticed, which are related to the symmetrical and asymmetric stretches of the groups $(SO_3)^-$. It is worth mentioning that the inorganic sulfate ions absorb strongly in 1125-1080 cm^{-1} due to the asymmetric stretching of S–O, while symmetrical stretching is normally prohibited by symmetry, but occasionally it can be seen as a very weak band around 1000 cm^{-1}. The bands that appear in the region from 670 to 584 cm^{-1} can be attributed to the metal-oxygen bond[41] as well as to the dye fragment after degradation with the Cu–J bond.

Conclusions

The $LaNiO_3$ material can be prepared by the modified proteic method using collagen as a chelating agent. The material presented $LaNiO_3$ phase with a perovskite structure and of rhombohedral geometry. This material has the presence of fine and porous particles, uniformly agglomerated with different pore sizes, a surface area of 22 $m^2\ g^{-1}$ and a value of $pH_{PCZ} = 7.44$. In the optimization of the best conditions to removal of Turquoise Blue dye, the mass of 50 mg of adsorbent and the acidic pH = 3.0 were the ones that presented the greatest efficiency. Regarding the application of the $LaNiO_3$ material as an adsorbent, it was found that the material showed removal efficiency greater than 88% for the removal of the Turquoise Blue dye in aqueous solution. Among the studied kinetic models, the experimental values were better adjusted to the model of variable constants, suggesting that the interaction processes undergo changes in the reaction mechanism and speed during the analyzed time, with the electrostatic attraction between the dye and the sites of the adsorbent surface being the predominant mechanism. The perovskite structure resisted the conditions of adsorption of the dye in aqueous medium, in addition to withstanding the high temperature of calcination used in the recovery of the adsorbent. The application of adsorption in cycles revealed the possibility of the LN-C9 adsorbent material being applied for 6 consecutive times without losing its dye removal effectiveness, maintaining high removal values of approximately 93%. The dye is decomposed during adsorbent recovery.

Supplementary Information

Supplementary data are available free of charge at http://jbcs.sbq.org.br as PDF file.

Acknowledgments

The authors acknowledge to PPGQ/UFS, CNPq and CAPES for its financial support. This study was financed in part by the Coordenação de Aperfeiçoamento de Pessoal de Nível Superior - Brazil (CAPES) - Finance Code 001 and to CLQM (Center of Multi-users Chemistry Laboratories) from Federal University of Sergipe for the analysis support.

References

1. Starling, M. C. V. M.; Leão, M. M. D.; Amorim, C. C.; *J. Hazard. Mater.* **2019**, *372*, 17. [Crossref]
2. Sousa, J. C. G.; Ribeiro, A. R.; Barbosa, M. O.; Pereira, M. F. R.; Silva, A. M. T.; *J. Hazard. Mater.* **2018**, *344*, 146. [Crossref]
3. Peixoto, F. P.; Marinho, G.; Rodrigues, K.; *Holos* **2013**, *5*, 98. [Crossref]
4. Acemioğlu, B.; *J. Colloid Interface Sci.* **2004**, *274*, 371. [Crossref]
5. Salem, V.; *Tingimento Têxtil: Fibras, Conceitos e Tecnologias*; Blucher Golden Tecnologia: São Paulo, 2010.
6. Tunç, O.; Tanaci, H.; Aksu, Z.; *J. Hazard. Mater.* **2009**, *163*, 187. [Crossref]
7. Martins, N.; Roriz, C. L.; Morales, P.; Barros, L.; Ferreira, I. C. F. R.; *Trends Food Sci. Technol.* **2016**, *52*, 1. [Crossref]
8. Guerra, E.; Rivera, G. A.; Lompart, M.; Jares, C. G.; *Talanta* **2018**, *188*, 251. [Crossref]
9. Qi, Y.; Yang, M.; Xu, W.; He, S.; Men, Y.; *J. Colloid Interface Sci.* **2017**, *486*, 84. [Crossref]
10. Anjos, F. S. C.; Vieira, E. F. S.; Cestari, A. R.; *J. Colloid Interface Sci.* **2002**, *253*, 243. [Crossref]
11. Machado, S. W. M.; Santos, C. D.; Souza, M. J. B.; Garrido Pedrosa, A. M.; *Sci. Plena* **2015**, *11*, 077201. [Crossref]
12. Schimmel, D.; Fagnani, K. C.; dos Santos, J. B. O.; Barros, M. A. S. D.; da Silva, E. A.; *Braz. J. Chem. Eng.* **2010**, *27*, 289. [Crossref]

13. Ramesh, K.; Rajappa, A.; Nandhakumar, V.; *Z. Phys. Chem.* **2017**, *231*, 1057. [Crossref]
14. Aguedal, H.; Iddou, A.; Locs, J.; *Key Eng. Mater.* **2018**, *762*, 81. [Crossref]
15. Jamil, F.; Asgher, M.; Hussain, F.; Bhatti, H. N.; *J. Anim. Plant Sci.* **2018**, *28*, 231. [Link] accessed in June 2022
16. Pardiwala, J. M.; Patel, F. J.; Patel, S. S.; *Int. J. Adv. Res. Eng. Technol.* **2017**, *8*, 8. [Link] accessed in June 2022
17. Silva, N. C. G.; Souza, M. C. M.; Silva Jr., I. J.; dos Santos, Z. M.; Rocha, M. V. P.; *Sep. Sci. Technol.* **2015**, *50*, 1616. [Crossref]
18. Tahir, M. A.; Bhatti, H. N.; Hussain, I.; Bhatti, I. A.; Asghar, M.; *Z. Phys. Chem.* **2020**, *234*, 233. [Crossref]
19. Sarioglu, O. F.; Keskin, N. O. S.; Celebioglu, A.; Tekinay, T.; Uyar, T.; *Chemosphere* **2017**, *184*, 393. [Crossref]
20. Melo, D. S.; Marinho É. P.; Soledade, L. E. B.; Melo, D. M. A.; Lima, S. J. G.; Longo, E.; Santos, I. M. G.; Souza, A. G.; *J. Mater. Sci.* **2008**, *43*, 551. [Crossref]
21. Moure, C.; Peña, O.; *Prog. Solid State Chem*. **2015**, *43*, 123. [Crossref]
22. Zhu, J.; Li, H.; Zhong, L.; Xiao, P.; Xu, X.; Yang, X.; Zhao, Z.; Li, J.; *ACS Catal.* **2014**, *4*, 2917. [Crossref]
23. Grabowska, E.; *Appl. Catal., B* **2016**, *186*, 97. [Crossref]
24. Hang, Y.; Si, Y.; Zhou, Q.; Yin, H.; Wang, A.; Cao, A.; *J. Hazard. Mater.* **2019**, *380*, 120789. [Crossref]
25. Liu, L.; Li, J.; Zhang, H.; Li, L.; Zhou, P.; Meng, X.; Guo, M.; Jia, J.; Sun, T.; *J. Hazard. Mater.* **2019**, *362*, 178. [Crossref]
26. Wu, Y.; Wang, H.; Tu, W.; Liu, Y.; Tan, Y. Z.; Yuan, X.; Chew, J. W.; *J. Hazard. Mater.* **2018**, *347*, 412. [Crossref]
27. Chu, Y.; Tan, X.; Shen, Z.; Liu, P.; Han, N.; Kang, J.; Duan, X.; Wang, S.; Liu, L.; Liu, S.; *J. Hazard. Mater*. **2018**, *356*, 53. [Crossref]
28. Siqueira, J. R. R.; Simões, A.; Stojanovic, B. D.; Paiva-Santos, C. O.; Longo, E.; Varela, J. A.; *Ceram. Int*. **2007**, *33*, 937. [Crossref]
29. Bolarín, A. M.; Sánchez, F.; Ponce, A.; Martínez, E. E.; *Mater. Sci. Eng., A* **2007**, *454-455*, 69. [Crossref]
30. Jadhav, A. L.; Khetre, S. M.; *Int. Nano Lett.* **2020**, *10*, 23. [Crossref]
31. Sellam, D.; Ikkour, K.; Dekkar, S.; Messaoudi, H.; Belaid, T.; Roger, A. C.; *Bull. Chem. React. Eng. Catal.* **2019**, *14*, 568. [Crossref]
32. Hu, Q.; Yue, B.; Shao, H.; Yang, F.; Wang, J.; Wang, Y.; Liu, J.; *J. Alloys Compd.* **2021**, *852*, 157002. [Crossref]
33. Wang, X.; Cao, W.; Qin, L.; Lin, T.; Chen, W.; Lin, S.; Yao, J.; Zhao, X.; Zhou, M.; Hang, C.; Wei, H.; *Theranostics* **2017**, *7*, 2277. [Crossref]
34. Bian, J.; Su, R.; Yao, Y.; Wang, J.; Zhou, J.; Li, F.; Wang, Z. L.; Sun, C.; *ACS Appl. Energy Mater.* **2019**, *2*, 923. [Crossref]
35. Farhadi, S.; Mahmoudi, F.; *Polyhedron* **2019**, *169*, 39. [Crossref]
36. Santos, A. G.; Leite, J. O.; Souza, M. J. B.; Gimenez, I. F.; Garrido Pedrosa, A. M.; *Ceram. Int.* **2018**, *44*, 5743. [Crossref]
37. Santos, A. G.; Leite, J. O.; Gimenez, I. F.; Souza, M. J. B.; Garrido Pedrosa, A. M.; *Mater. Res. Express* **2019**, *6*, 105065. [Crossref]
38. Santiago, P.; Lima, C. C.; Bott-Neto, J. L.; Fernández, P.; Angelucci, C. A.; Garcia, J. S.; *J. Electroanal. Chem.* **2021**, *896*, 115198. [Crossref]
39. Hu, K.; Ding, W.; Wang, S.; Li, Q.; Zhang, M.; Huang, F.; Kong, X.; Liu, Q.; *J. Alloys Compd.* **2020**, *848*, 156579. [Crossref]
40. Braga, T. P.; Dias, D. F.; de Sousa, M. F.; Soares, J. M.; Sasaki, J. M.; *J. Alloys Compd.* **2015**, *622*, 408. [Crossref]
41. Santos, J. C.; Souza, M. J. B.; Ruiz, J. A. C.; Melo, D. M. A.; Mesquita, M. E.; Garrido Pedrosa, A. M.; *J. Braz. Chem. Soc.* **2012**, *23*, 1858. [Crossref]
42. Palas, B.; Ersoz, G.; Atalay, S.; *Chemosphere* **2018**, *209*, 823. [Crossref]
43. Karthikeyan, C.; Thamima, M.; Karuppuchamy, S.; *Mater. Today: Proc.* **2021**, *35*, 44. [Crossref]
44. Karami, M.; Ghanbari, M.; Amiri, O.; Salavati-Niasari, M.; *Sep. Purif. Technol.* **2020**, *253*, 117526. [Crossref]
45. Phan, T. T. N.; Nikoloski, A. N.; Bahri, P. A.; Li, D.; *Appl. Surf. Sci.* **2019**, *491*, 488. [Crossref]
46. Tavakoli-Azar, T.; Mahjoub, A. R.; Sadjadi, M. S.; Farhadyar, N.; Sadr, M. H.; *Inorg. Chem. Commun.* **2020**, *119*, 108091. [Crossref]
47. Manjunatha, C. R.; Nagabhushana, B. M.; Raghu, M. S.; Pratibha, S.; Dhananjaya, N.; Narayan, A.; *Mater. Sci. Eng., C* **2019**, *101*, 674. [Crossref]
48. Deng, H.; Mao, Z.; Xua, H.; Zhang, L.; Zhong, Y.; Sui, X.; *Ecotoxicol. Environ. Saf.* **2019**, *168*, 35. [Crossref]
49. Farhadi, S.; Mahmoudi, F.; Amini, M. M.; Dusek, M.; Jarosova, M.; *Dalton Trans.* **2017**, *46*, 3252. [Crossref]
50. Huerta-Flores, A. M.; Sánchez-Martínez, D.; Hernández-Romero, M. R.; Zarazúa-Morín, M. E.; Torres-Martínez, L. M.; *J. Photochem. Photobiol., A* **2019**, *368*, 70. [Crossref]
51. Brinker, C. J.; Scherrer, G. W.; *Sol-Gel Science the Physics and Chemistry of Sol-Gel Processing*; Academic Press, INC: New York, 1990.
52. Larson, A.; Von Dreele, R.; *General Structure Analysis System (GSAS), Report LAUR 86-748*; Los Alamos National Laboratory, USA; [Link] Rietveld, H.; *J. Appl. Crystallogr.* **1969**, *2*, 65. [Crossref]
53. Scherrer, P.; *Math-Phys* Kl **1918**, *1918*, 98.
54. Kissinger, H. E.; *Anal. Chem.* **1957**, *29*, 1702. [Crossref]
55. Lemos, J. A. S.; Souza, V. M. S. C.; Ribeiro, I. A.; Souza, M. J. B.; Pedrosa, A. M. G. In *Anais do 13th Brazillian Meeting on Adsorption*; de Azevedo, D. C. S.; Bastos-Neto, M., eds.; Imprensa Universitária: Fortaleza, 2021, p. 59. [Link] accessed in June 2022
56. Guo, J.; Khan, S.; Cho, S.; Kim, J.; *Appl. Surf. Sci.* **2019**, *473*, 425. [Crossref]

57. Ahmad, M. A.; Afandi, N. S.; Adegoke, K. A.; Bello, O. S.; *Desalin. Water Treat.* **2016**, *57*, 21487. [Crossref]
58. Simonin, J. P.; *Chem. Eng. J.* **2016**, *300*, 254. [Crossref]
59. Wang, L.; Li, J.; Wang, Y.; Zhao, L.; *J. Hazard. Mater.* **2011**, *196*, 342. [Crossref]
60. Aquino, F. M.; Melo, D. M. A.; Pimentel, P. M.; Braga, R. M.; Melo, M. A. F.; Martinelli, A. E.; Costa, A. F.; *Mater. Res. Bull.* **2012**, *47*, 2605. [Crossref]
61. Riaz, T.; Zeeshan, R.; Zarif, F.; Ilyas, K.; Muhammad, N.; Safi, S. Z.; Rahim, A.; Rizvi, S. A. A.; Rehman, I. U.; *Appl. Spectrosc. Rev.* **2018**, *53*, 703. [Crossref]
62. Haron, W.; Wisitsoraat, A.; Sirimahachai, U.; Wongnawa, S.; Songklanakarin, J.; *J. Sci. Technol.* **2018**, *40*, 484. [Link] accessed in June 2022
63. Moraes Jr., E. O. M.; Leite, J. O.; Santos, A. G.; Souza, M. J. B.; Garrido Pedrosa, A. M.; *Cerâmica* **2018**, *64*, 436. [Crossref]
64. Oliveira, F. S.; Pimentel, P. M.; Oliveira, R. M. P. B.; Melo, D. M. A.; Melo, M. A. F.; *Mater. Lett.* **2010**, *64*, 2700. [Crossref]
65. Pavia, D. L.; Lampman, G. M.; Kriz, G. S.; Vyvyan, J. R.; *Introdução à Espectroscopia*, 4th ed.; Cengage Lelimarning: São Paulo, Brazil, 2010.
66. Zhao, M.; Yuan, Q.; Zhang, H.; Li, C.; Wang, Y.; Wang, W.; *J. Alloys Compd.* **2019**, *782*, 1049. [Crossref]
67. Oliveira, S. P.; Silva, W. L. L.; Viana, R. R.; *Cerâmica* **2013**, *59*, 338. [Crossref]
68. Cunico, P.; Kumar, A.; Fungaro, D. A.; *J. Nanosci. Nanoeng*. **2015**, *1*, 148. [Link] accessed in June 2022
69. Coelho, G. F.; Celso Jr., A. C. G.; Sousa, R. F. B.; Schwantes, D.; Miola, A. J.; Domingues, C. V. R.; *J. Agron. Sci.* **2014**, *3*, 291.
70. Barcellos, I. O.; de Lima, T.; Blosfeld, A. M.; *Ecletica Quim.* **2013**, *38*, 176. [Crossref]

Submitted: February 24, 2022
Published online: June 14, 2022